Three-dimensional numerical simulation of crown spike due to coupling effect between bubbles and free surface*

Han Rui(韩 蕊), Zhang A-Man(张阿漫)†, and Li Shuai(李 帅)

College of Shipbuilding Engineering, Harbin Engineering University, Harbin 150001, *China*

(Received 26 May 2013; revised manuscript received 28 July 2013; published online 26 January 2014)

The motion of gas bubbles beneath a free surface will lead to a spike of fluid on the free surface. The distance of the bubbles to the free surface is the key factor to different phenomena. When the inception distance varies in some range, crown phenomenon would happen after the impact of weak buoyancy bubbles, so this kind of spike is defined as crown spike in the present paper. Based on potential flow theory, a three-dimensional numerical model is established to simulate the motion of the free-surface spike generated by one bubble or a horizontal line of two in-phase bubbles. After the downward jet formed near the end of the collapse phase, the simulation of the free surface is performed to study the crown spike without regard to the toroidal bubble's effect. Calculations about the interaction between one bubble and free surface agree well with the experimental results conducted with a high-speed camera, and relative error is within 15%. Crown spike in both single- and two-bubble cases are simulated numerically. Different features and laws of the motion of crown spike, depending on the bubble-boundary distances and the inter-bubble distances, have been investigated.

Keywords: bubble, free surface, three-dimensional numerical model, crown spike

PACS: 47.55.dd, 47.55.dr, 47.11.Hj **DOI:** 10.1088/1674-1056/23/3/034703

1. Introduction

Bubble dynamics has become an important research field for decades, owing to a wide range of applications of bubbles, such as gas bubble gun used for detecting oil in the field of ocean engineering, bubble for drag and noise reduction of ocean vessels, and the jet of bubble towards rigid wall to remove dirt from precision instruments and to remove calculus in medical treatment. In addition, we are concerned about high-speed jet formed by explosion bubble towards ships. Owing to all the factors above, research on the bubble behavior has been made extensively. More complex physical phenomena occur when the free surface provides a boundary to bubble. Experimental observations by Gibson,[1] Chahine,[2] and Blake & Gibson[3] showed that a liquid jet directed away from the free surface is formed by weak buoyancy bubbles near the end of collapse phase while the free surface produces a spike that moves upward. A boundary element method or a boundary integral method, which has been verified repeatedly,[3–6] has been widely used to calculate the nonlinear motion of bubbles near different boundaries. For example, the interaction between one bubble and the free surface is studied by Wang,[7] where both effects of buoyancy and bubble-boundary distances on bubbles are addressed. To study the physical phenomena after the jet impact of bubbles, Wang[8] introduced a vortex ring to simulate the motion features of toroidal bubbles. However, the fact that toroidal bubbles collapse in a short time challenges continued calculation. With increasing concern about underwater explosion in the military field, Zhang *et al.*[9] numerically simulated the whole process of an underwater explosion based on SPH and BEM combination, but without a free surface. There are a number of studies about the interaction between two-bubble and free surface. The work by Tomita and Kodama,[10] Robinson *et al.*,[11] and Pearson *et al.*[12] utilized lasers to produce both a single bubble and two bubbles in a vertical column beneath a free surface, studying different types of bubble behavior. In conclusion, the motion of bubbles is always of high interest, rather than the motion of free-surface spike after bubbles form a liquid jet. However, the free-surface spike starts to draw attention due to the application of splashes from underwater explosions as water barrier.[13,14]

Aiming to study the spike generated by bubbles, the liquid spike of the free surface is well modeled by a Dirichlet hyperbolic in the paper of Longuet-Higgins,[15] and calculation results are found to agree well with the experimental observations by Blake and Gibson.[3] Different motions of violent surface were given by Rogers and Szymczak.[16] Spark-generated bubbles near the free surface are observed by Zhang *et al.*[17] with a high-speed camera to study vastly different phenomena. They discovered a special phenomenon that a circle of the outer fluid would appear quickly to surround the middle water column in some cases. A landmark progress of understanding this phenomenon is from Li *et al.*,[18] where an axisymmetric model is established to investigate the effects of parameter variation on spike patterns. Nevertheless, such phenomenon

*Project supported by the Major Basic Research Project of National Security of China (Grant No. 613157) and the Excellent Young Scientists Fund of China (Grant No. 51222904).

†Corresponding author. E-mail: zhangaman@hrbeu.edu.cn

© 2014 Chinese Physical Society and IOP Publishing Ltd

would happen in the formation process of both crown spike and tower spike. Hence, a circle of the outer fluid, the phenomenon and spikes above are defined as crown, crown phenomenon, and crown spike in this paper, respectively, distinguished from Ref. [17]. Although it is possible to simulate numerically the motion before toroidal bubbles collapse, there are few studies[18] about crown phenomenon because it happens a long time after the impact of bubbles.

The crown spike is studied in this paper. Followed by Ref. [18], a three-dimensional (3D) numerical model is first established to simulate the interaction between bubbles and free surface with a boundary element method, and then the motion of the free-surface spike is further simulated[19–21] after weak buoyancy bubbles form downward jet so as to avoid the difficulty of simulating toroidal bubbles. The numerical approach mentioned above is used to deal with single- and two-bubble cases, and then laws of the free-surface motion are summarized. Nevertheless, physical phenomena like crown extension and droplet come-off would happen afterwards (see Figs. 1 and 2). Then, we numerically simulate the beginning of crown extension process because the limitations of the 3D grids cannot be well solved and droplet come-off is hard to handle with a boundary element method, aiming to provide information for studying the crown phenomenon.



Fig. 1. Crown extension.



Fig. 2. Droplet come-off.

2. Experimental setup

The details of the experimental arrangement and method can be found in Ref. [17]. This section will give a brief description of the procedure. Experimental setup includes a 200-V dc supply used to generate spark bubble, an open-top water tank, a light source, and a high-speed camera. The tank filled with fresh water is a transparent water gullet with size of $500\times500\times500$ mm^3. The light source is continuous with a power rating of 55 kW. The high-speed camera (Phantom V12.1) operates at 6242 frames per second with the maximum resolution. Fine copper wires with a diameter of about 0.013 mm are used as electrodes in series to generate in-phase bubbles. Switch K1 and switch K2 are responsible for charging and discharging the electricity, respectively. At the beginning, switch K1 is turned on to charge a 6600 μF capacitor till an expected voltmeter reading is reached. Next, the camera is turned on at the same time when the switch K2 is turned on for electrical discharge, and then copper wires burn in a short time to vaporize surrounding fluid for generating bubbles. When the experiment is over, we turn off the switch K2 and the camera successively.

3. Theory and numerical modeling

3.1. Theory

Based on potential flow theory, a 3D numerical model is established to simulate the physical phenomenon in this paper. Due to the small velocity of the bubble wall compared to the sound speed in the liquid, the large Reynolds numbers, and the short duration of the motion, the flow is assumed to be incompressible, inviscid, and irrotational, and thus the velocity potential satisfies the Laplace equation and the boundary integral equation[22]

$$\nabla^2\Phi = 0, \tag{1}$$

$$\vartheta\Phi(\boldsymbol{p}) = \iint_S \left(\frac{\partial\Phi(\boldsymbol{q})}{\partial\boldsymbol{n}}G(\boldsymbol{p},\boldsymbol{q}) - \Phi(\boldsymbol{q})\frac{\partial}{\partial\boldsymbol{n}}G(\boldsymbol{p},\boldsymbol{q})\right)\mathrm{d}S, \tag{2}$$

where S is all the boundaries of the fluid domain, $\boldsymbol{p}$ and $\boldsymbol{q}$ are the fixed point and the source point located at the interface, $G(\boldsymbol{p},\boldsymbol{q}) = 1/|\boldsymbol{r}(\boldsymbol{p})-\boldsymbol{r}(\boldsymbol{q})|$ is the Green's function, ϑ is the solid angle at fixed point $\boldsymbol{p}$ which equals 2π, and $\boldsymbol{n}$ is the outward normal with the definition of the normal derivative as $\partial/\partial\boldsymbol{n} = \boldsymbol{n}\cdot\nabla$.

Pressure on both sides of the bubble wall is equal, and the pressure within the bubble is assumed to be related to the initial state and its volume without regard to the influence from the motion of the gas inside the bubble during its expansion and compression. Therefore, the liquid pressure outside the bubble wall can be written as[8]

$$P = P_{\mathrm{c}} + P_0\left(\frac{V_0}{V}\right)^k, \tag{3}$$

where P_c is the constant vapor pressure inside the bubble, P_0 and V_0 are the initial pressure and volume of the bubble, and k is the ratio of the specific heat for the gas related to gas component and equal to 1.25, which is favorable for the underwater explosion bubble and the spark-generated bubble in this paper.[19,23]

Incompressible ideal fluid in unsteady irrotational flow domain satisfies the following equation:

$$\frac{\partial \Phi}{\partial t}+\frac{\boldsymbol{u}^2}{2}+\frac{P}{\rho}+gz=\frac{P_\infty}{\rho}, \tag{4}$$

where ρ is the density of the fluid, g is the acceleration due to gravity, z is the vertical component of the position vector, and P_∞ represents the hydrostatic pressure at the level of the bubble centre at inception. With the relation $\boldsymbol{u}=\nabla\Phi$ in the flow domain, the total derivative

$$\frac{\mathrm{d}\Phi}{\mathrm{d}t}=\frac{\partial \Phi}{\partial t}+\boldsymbol{u}\cdot\nabla\Phi=\frac{\partial \Phi}{\partial t}+|\boldsymbol{u}|^2$$

is substituted into Eq. (4). Then we scale length, pressure, time, velocity potential, and buoyancy with respect to R_m, P_{ref}, $R_m(\rho/P_{ref})^{1/2}$, $R_m(P_{ref}/\rho)^{1/2}$, and $(\rho g R_m/P_{ref})^{1/2}$, respectively. Here, R_m is the maximum radius that the bubble would achieve in an infinite flow domain, and P_{ref} is defined as $P_{ref}=P_\infty-P_c$.[24] The state equations of the bubble and free surface can be respectively transformed into[8]

$$\frac{\mathrm{d}\Phi}{\mathrm{d}t}=1+\frac{|\boldsymbol{u}|^2}{2}-\delta^2 z-\varepsilon\left(\frac{V_0}{V}\right)^k,$$

(for the bubble surface), (5a)

$$\frac{\mathrm{d}\Phi}{\mathrm{d}t}=\frac{|\boldsymbol{u}|^2}{2}-\delta^2(z-\gamma_f),$$

(for the free surface), (5b)

where the dimensionless parameters are defined as: the buoyancy parameter $\delta=\sqrt{\rho g R_m/P_{ref}}$; the strength parameter inside the bubble $\varepsilon=P_0/P_{ref}$; the dimensionless distance of the bubble from the free surface $\gamma_f=d/R_m$; and d is the initial distance of the bubble centroid from the free surface. For two-bubble cases, we define the dimensionless inter-bubble distance as $b=B/R_m$ and the distance between the initial bubble centroid as B.

The kinematic boundary condition governing the motion of the bubble and the free surface is[8]

$$\frac{\mathrm{d}\boldsymbol{r}}{\mathrm{d}t}=\boldsymbol{u}, \tag{6}$$

where $\boldsymbol{r}$ denotes the spatial position of the fixed point $\boldsymbol{p}$ on the bubble surface or the free surface.

3.2. Numerical implementation

For a more detailed procedure to solve Eq. (2), we can refer to Ref. [25]. First of all, the bubble and the free surface with a radius of 4.5[26] are discretized into M small triangular elements and N nodes (see Fig. 3(a)) and it can be found in Fig. 3(a) that finer grids are used in the central two thirds of the free surface for a high degree of accuracy. Take the m-th element $\Delta A_m B_m C_m$ as an example to explain the procedure, it should be transformed into a unit right triangle $A'_m B'_m C'_m$ for calculation with the Jacobian of the transformation $\mathrm{J}=\left|(\boldsymbol{r}_{A'_m}-\boldsymbol{r}_{B'_m})\times(\boldsymbol{r}_{A'_m}-\boldsymbol{r}_{C'_m})\right|$, as illustrated in Fig. 3(b), so the geometric position function of the source point $\boldsymbol{r}(\boldsymbol{q})$, the velocity potential function $\Phi(\boldsymbol{q})$, and the normal component of the velocity $\psi(\boldsymbol{q})=\partial\Phi(\boldsymbol{q})/\partial n$ can be obtained by linear interpolation.

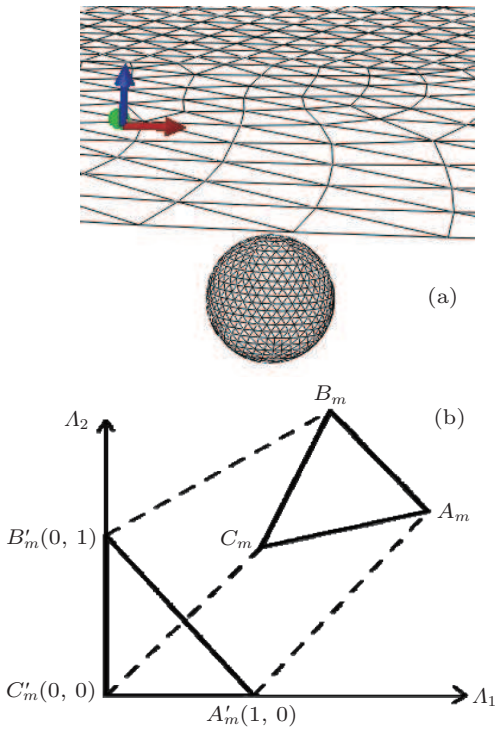


Fig. 3. (color online) (a) Discretized bubble and free surface. (b) Element coordinate mapping.[25]

The integral of the two terms on the right-hand side in Eq. (2) over the m-th element can be expressed, respectively, as follows:

$$\overline{G}=\int_0^1\int_0^{1-\Lambda_2}\frac{\mathrm{J}\,\mathrm{d}\Lambda_1\,\mathrm{d}\Lambda_2}{|\boldsymbol{r}(\boldsymbol{p})-\boldsymbol{r}(\boldsymbol{q})|}\cdot\psi(\boldsymbol{q}), \tag{7}$$

$$\overline{H'}=\int_0^1\int_0^{1-\Lambda_2}\frac{\partial}{\partial n}\left(\frac{1}{|\boldsymbol{r}(\boldsymbol{p})-\boldsymbol{r}(\boldsymbol{q})|}\right)\mathrm{J}\,\mathrm{d}\Lambda_1\,\mathrm{d}\Lambda_2\cdot\Phi(\boldsymbol{q}). \tag{8}$$

We add up the integral results over all elements, thus obtaining a linear equation of $\Phi(\boldsymbol{p})$. By carrying out the same calculations for all the nodes, we obtain a system of N linear equations in the following form:

$$\boldsymbol{H}\cdot\boldsymbol{\Phi}=\boldsymbol{G}\cdot\psi. \tag{9}$$

The off-diagonal elements of the matrix $\boldsymbol{G}$ and $\boldsymbol{H}$ are solved by using seven-point Gaussian quadrature in this paper, while the diagonal elements should be dealt with because of

the singularities. Weak and strong singularity appear on the influence coefficient G_{ii} and H_{ii}, respectively. A traditional method is used to solve the problem.[27,28]

In our calculations, we discretize the time domain. In order to maintain the stability of the calculation process, every time-step size must be carefully controlled so as to bound the changes in the velocity potential at each time. In the present paper, Δt is chosen according to Eq. (5) so that the change in Φ at each node can be smaller than $\Delta\Phi$, which is kept to be 0.03 before the jet and 0.01 after the jet.

In order to calculate the motion of the free-surface spike, the process of the simulation is divided into two parts: the motion of both the bubble and the free surface is simulated before the jet impact; the free surface is further simulated without regard to the effect of the toroidal bubble after the jet impact, then the crown spike is obtained. Detailed explanations for the numerical method above will be given in Section 3.3.

3.3. Numerical model for the simulation of crown spike

There is little progress in the simulation of the free-surface motion after the jet impact, the main reason for which is that the toroidal bubble would collapse for a short period,[8] and therefore the method suggested in Section 3.2 is adopted in this paper to avoid the challenge of simulating the toroidal bubble.

Because of difficulties in simulating the toroidal bubble motion, the method of ignoring the effect of the toroidal bubble has been used in many previous studies.[19–21] We take the previous numerical method as a reference. The same approach is adopted in this paper and the main reasons are described as follows. The energy loss probably occurs at the moment when the minimum volume of the bubble is reached and the total energy in the second cycle is about 30% of that in the first cycle for explosion-generated and spark-generated bubbles.[23,29,30] A downward jet is formed by weak buoyancy bubbles when the distance parameter $\gamma_f \in [0.6, 1.2]$, which leads to a large amount of energy loss, and then the toroidal bubble after the jet would quickly move downward and continue to collapse for a short period, while the crown phenomenon does not occur, as depicted in Fig. 4. Both the motion and the collapse would lead to great energy loss again. The interaction between the toroidal bubble and the free surface were calculated in Ref. [8], and the bubble in toroidal form would continue to collapse for a short period in which the free surface moved only slightly for $\gamma_f = 1.0$. However, the free surface may go up significantly for $\gamma_f < 0.5$. Because of the limitations of both the method and the numerical model, crown spike of the free surface generated by the bubble initiated at $\gamma_f \in [1.0, 1.2]$ is investigated. With the increase in the distance parameter, the influence of the bubble on the free surface decreases, so it is assumed that the conclusion of Ref. [8] applies to the cases in which the range of γ_f is $[1.0, 1.2]$. In summary, it can be assumed that the interaction between the bubble and the free surface becomes weaker rapidly after the jet impact, while the free surface continues to move upward due to inertia, so the effect of the toroidal bubble is ignored after the jet impact to avoid the challenge in numerical calculations. To ascertain the validity of the handling method in the present paper, comparison between the experimental phenomena and the numerical results is made. If both the spike shapes and the motion trends are in accordance and the relative errors are within permission, the method in this paper can be considered effective to study the spike phenomena.

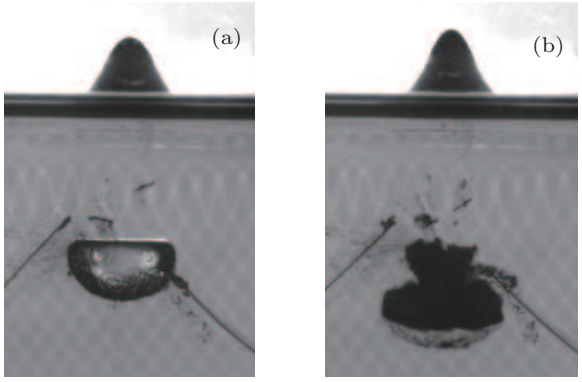


Fig. 4. (a) Immediately before impact at T = 2.816 ms. (b) Break-up of the toroidal bubble at T = 3.256 ms. $\gamma_f \approx 1.0$ with a maximum bubble radius of 12.44 mm.

4. Coupling effect between bubbles and free surface

The spike phenomena after impact in both single- and two-bubble cases are investigated in this paper, and we should define some parameters related to the crown spike, as depicted in Fig. 5.

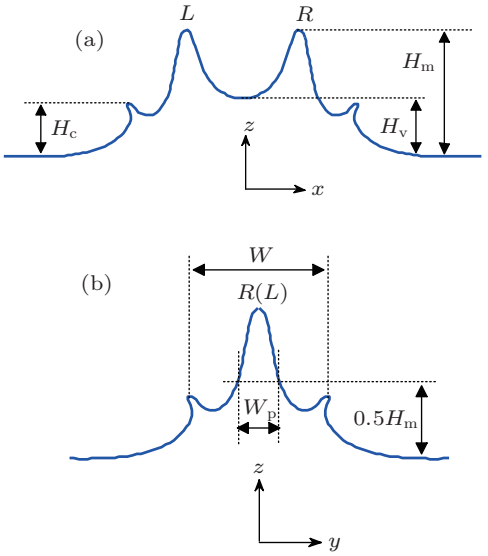


Fig. 5. (color online) (a) Front view and (b) side view of 3D crown spike.

In the following discussion, as shown in Fig. 5(a), the high water column is defined as the main peak of the spike, and there are two main peaks in two-bubble case, which are defined as left peak and right peak, respectively. A circle of the outer rising fluid is defined as the crown of the spike. The distance of the peak tip from the distant quiescent water surface is called peak height, expressed by H_{m}. We call the portion between the two peaks valley and the distance of its bottom from the distant quiescent water surface is defined as valley height, expressed as H_{v}. The distance of the crown apex from the faraway quiescent water surface is expressed by H_{c}, called crown height. As depicted in Fig. 5(b), the maximum width of the crown along the y axis is crown width, expressed by W. To describe the evolution of spike phenomena, we define the peak width along the y axis at the height of $0.5H_{\mathrm{m}}$ as peak width, expressed as W_{p}.

A three-dimensional model is established in the numerical simulation with the free surface discretized into 7792 triangular elements and the bubble into 1280 triangular elements. A second-order Runge-Kutta scheme is adopted and the time-step size is carefully controlled as stated in Section 3.2.

4.1. Comparison of the experimental data and 3D numerical results

To validate the numerical model, 3D numerical results are compared with the experimental data. The maximum radius of

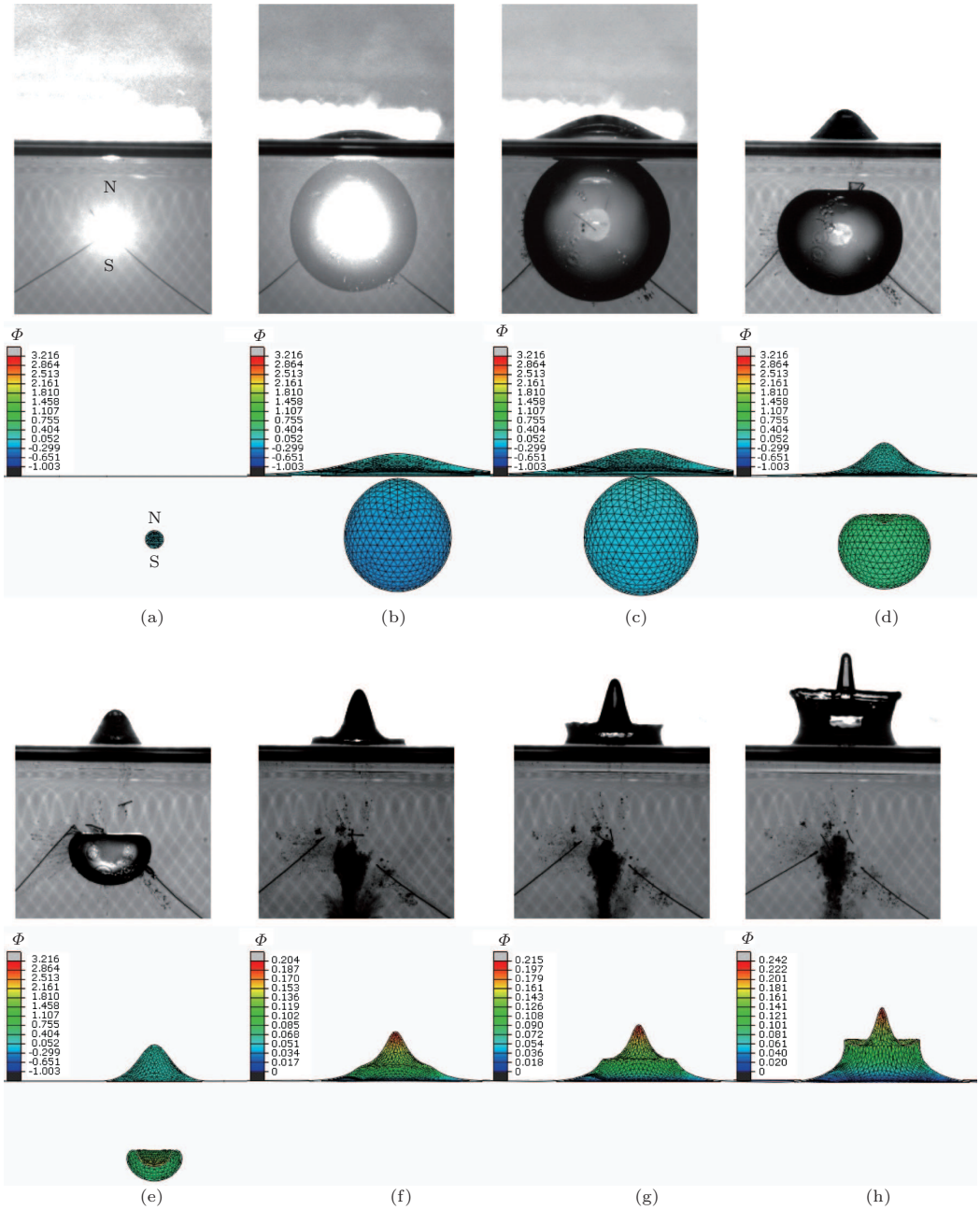


Fig. 6. (color online) Comparison between the experimental and numerical results at (a) $T = 0$ ms, (b) $T = 0.968$ ms, (c) $T = 1.496$ ms, (d) $T = 2.288$ ms, (e) $T = 2.728$ ms, (f) $T = 4.576$ ms, (g) $T = 5.544$ ms, and (h) $T = 8.096$ ms.

the spark-generated bubble in the experiment is 12.27 mm and the bubble is initiated at 12.87 mm from the free surface with a value of $\gamma_f \approx 1.05$. Comparison between the experimental and numerical results is shown in Fig. 6.

The bubble and free-surface profiles before impact are shown in Figs. 6(a)–6(e) and the spike phenomena after impact are shown in Figs. 6(f)–6(h), in which the potential contours of the fluid domain in numerical results are dimensionless. A tiny high-pressure bubble is formed with the definitions of north pole and south pole (Fig. 6(a)), and then it begins to expand. At $T = 0.968$ ms, the free surface is slightly elevated by the expansion of the bubble, which indicates the initial formation of the spike, and the bubble is slightly elongated along the z axis in Fig. 6(b). At $T = 1.496$ ms, the maximum volume of the bubble is reached and its top half becomes entrained into the base of the rising free surface, leading to a larger hump in Fig. 6(c). At $T = 2.288$ ms, the bubble comes into the collapse phase and a downward jet is formed with the bubble upper surface moving down, and the spike continues to rise along the symmetric axis with decreasing width of the spike base at the same time, evolving into a slim spike in Fig. 6(d). At $T = 2.728$ ms, the spike evolves in the same way as that in Fig. 6(e), the bubble jet is promoted by the presence of the free surface, and the motion of the toroidal bubble would proceed with neither evident rebounding phenomenon nor clear outline of the bubble, which indicates a large amount of energy loss and less influence of the bubble on the free surface. The profile of the spike at $T = 4.576$ ms is shown in Fig. 6(f), and the crown phenomenon appears around the slimmer peak. At $T = 5.544$ ms, the crown phenomenon becomes more evident with a significant increase in height of the crown (see Fig. 6(g)). The height of the spike further increases at $T = 8.096$ ms in Fig. 6(h). The experimental and numerical results of the impact time T_j and the crown spike parameters at $T = 8.096$ ms are compared in Table 1 and the relative errors are also listed.

Table 1. Relative errors between the experimental and numerical results.

	T_j/ms	H_m/mm	H_c/mm	W/mm
Experimental data	2.816	16.36	9.89	18.07
Numerical results	2.898	15.11	8.44	15.62
Relative errors/%	2.91	7.64	14.66	13.56

By comparing the experimental phenomena with the numerical calculations, a good agreement is observed both before and after the impact, since both the spike shapes and the motion trends are in accordance and the relative error of the impact time is within 3%, which reveals the precision of the model based on BEM to simulate the interaction between bubbles and free surface in this paper. After impact, the relative errors of the crown spike parameters are all within 15%. The reasons for the error are given below: (i) the fluid viscosity and the surface tension are not considered; (ii) the influence of the bubble on the free surface is ignored after the impact; (iii) the initial condition in the numerical calculations makes a difference in the results. However, in general, the validity of the model to simulate the crown spike has been confirmed in this paper. The simplified model is used in the following discussion to investigate the crown spike generated by a single bubble and a horizontal line of two bubbles in this paper.

4.2. Single-bubble cases

Single-bubble cases are studied first to investigate the effect of the distance parameter on the evolution of crown spike, with $\varepsilon = 100$, $R_0 = 0.1485$, $\delta^2 = 0.0036$, $\gamma_f = 1.0$, 1.1, and 1.2. To calculate the cases with different γ_f, the corresponding impact time is 1.581, 1.617, and 1.641. We note that the impact time increases with the increase in γ_f. The dimensionless times are selected due to the phenomena in case of $\gamma_f = 1.0$. The dimensionless times are the time of impact, the time of clear formation of the crown, the moment when the crown just rises to the level parallel to the distant quiescent water surface, and the moment $T' = 4$. The forms of crown spike with different γ_f are compared in Fig. 7.

At $T' = 1.581$, the broad jet impacts on the lower wall of the bubble in case of $\gamma_f = 1.0$, while the jets in other two cases are not complete. However, the downward jet in case of $\gamma_f = 1.1$ goes further than that in case of $\gamma_f = 1.2$, as shown in Fig. 7(a). There are two main reasons for the difference in the impact time. (i) With the increase in γ_f, the velocity of the north pole in expansion phase decreases more because of smaller gradient difference of pressure and larger mass of fluid above it (see Fig. 8), leading to a longer expansion phase, and naturally a later impact moment. (ii) During the collapse phase, fluid from sides is rapidly drawn into the region between bubble and the free surface, leading to the formation of a stagnation point along the symmetric axis. It can be seen that a high-pressure region is formed, which can redirect the incoming fluid to form the downward jet and the upward spike.[6] Based on the explanation above, nearly the same volume of the fluid drawn can be expected at the beginning of the collapse phase. It is clear that the increase in γ_f will cause smaller velocity of the incoming flow and that the pressure in the high-pressure region is lower so as to make it longer to complete the jet. In summary, the coupling effect between bubble and free surface weakens with the increase in γ_f, leading to the later impact moment and the lower velocity of the jet (see Fig. 8, the velocity curves of the south pole are nearly coincident in the whole process, while the collapsing velocity V_b of the north pole increases with decreasing γ_f). Accordingly, a smaller height and a wider base of the spike are formed. The evolution of the spike after the impact is illustrated in Figs. 7(b) and 7(c).

It is observed that the free surface continues to rise along the symmetric axis in all cases with contraction in the peak width. Crown phenomenon in case of $\gamma_f = 1.0$ is the earliest to occur. At $T' = 2.925$, the crown in case of $\gamma_f = 1.0$ just rises to the level parallel to the distant quiescent water surface, and crown phenomenon can be seen evidently in case of $\gamma_f = 1.1$ and just occurs in case of $\gamma_f = 1.2$. As shown in Fig. 9, the variation of crown height H_c with time in all cases increases linearly. We note that the time when crown phenomenon can be observed comes later for bubbles formed further away from the free surface with a greater initial crown height but a slower growth rate of crown height. At $T' = 4$ in Fig. 7(d), the main peak and the crown both arise in all cases. However, the successive ascent of the crown only in case of $\gamma_f = 1.0$ makes a groove between the main peak and the outer-extension crown, which indicates a larger crown width, as depicted in Fig. 10. Observing the corresponding variation of crown width, the crown width W decreases first and then increases in the case of $\gamma_f = 1.0$ and $\gamma_f = 1.1$, for the reason that the crown width diminishes together with the contraction in the peak width after the impact, while the peak width does not contract significantly with $\gamma_f = 1.2$, so the reduction of the crown width does not happen. By comparing the ascending sections of the curves, it is obvious that the crown width W increases slower and the crown phenomenon is less obvious with greater γ_f.

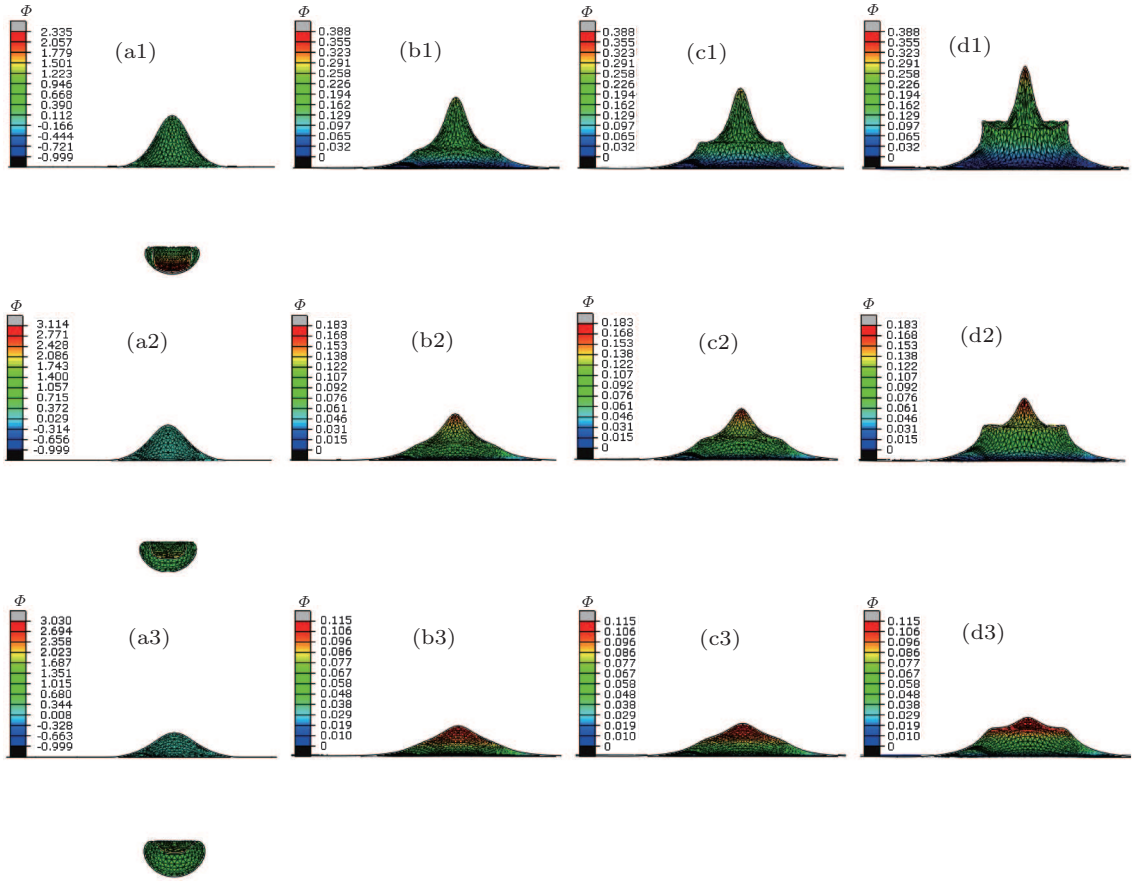


Fig. 7. (color online) Crown forms at the dimensionless time (a) $T' = 1.581$, (b) $T' = 2.487$, (c) $T' = 2.925$, and (d) $T' = 4$ with different γ_f.

Through comparing the spike forms above, we note that the time difference for the same phenomenon is due to the coupling effect between bubble and free surface, which means the difference in the free-surface velocity is obtained. There are two reasons for the velocity difference. First, the free-surface velocity obtained at the expansion phase differs due to the difference in the pressure gradient between bubble and free surface. Second, as mentioned above, different high-pressure regions will be formed at the collapse phase with different γ_f, thus free surface gains different velocities.

The variation of peak height H_m with time in all cases is shown in Fig. 11. It can be seen that the vertical velocity of the peak tip moving upward increases with the reduction of γ_f and the corresponding peak height is greater at that instant. The peak height increases rapidly in the expansion phase in all cases, but only the peak height in case of $\gamma_f = 1.2$ descends a little during the collapse phase, and the reason is given below. The spike tip with a small initial upward velocity starts to

decrease by gravity when the expansion of the bubble decelerates at the later stage of the expansion phase, and the bubble remains roughly spherical at the beginning of the collapse phase, so high pressure is not formed and the upward velocity of the spike tip becomes negative because of the continuous decrease. This is the reason why the main peak height descends a little. The high-pressure region is gradually formed as the collapse of the bubble progresses, which leads to the continuous increase in the upward velocity of the tip, and then the peak height $H_{\rm m}$ grows in linearity in a short time after the impact.

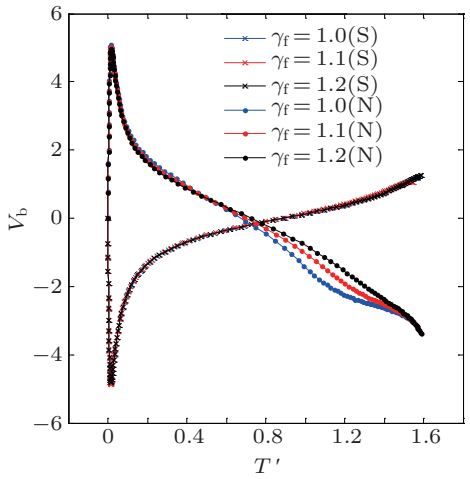


Fig. 8. (color online) Vertical velocities with different $\gamma_{\rm f}$.

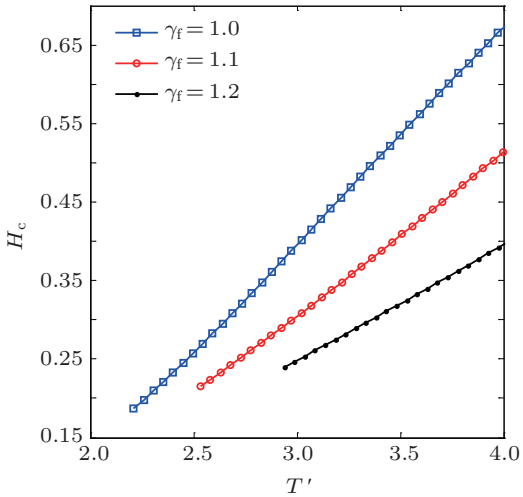


Fig. 9. (color online) Crown heights with different $\gamma_{\rm f}$.

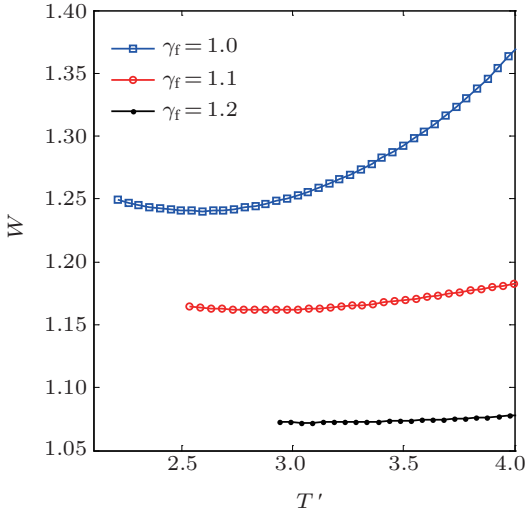


Fig. 10. (color online) Crown width with different $\gamma_{\rm f}$.

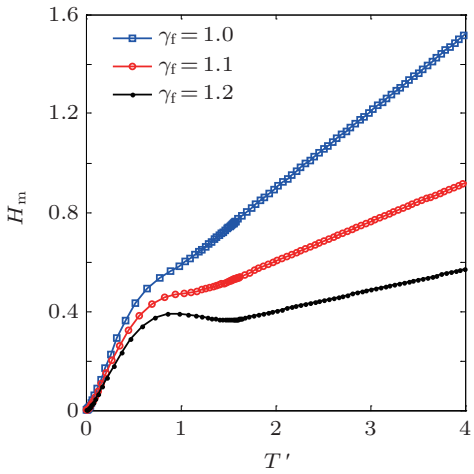


Fig. 11. (color online) Peak heights with different $\gamma_{\rm f}$.

4.3. Two-bubble cases

To study the crown spike induced by a horizontal line of two in-phase bubbles, five cases are computed in this paper, all with $\varepsilon = 100$, $R_0 = 0.1485$, and $\delta^2 = 0.0036$. In the first part, computations are carried out for bubbles initiated at $1.0R_{\rm m}$ from the free surface with different inter-bubble distances. In the second part, the distance parameter changes with the inter-bubble distance fixed at the value of $1.6R_{\rm m}$. There will be a valley between the two peaks in two-bubble cases, the valley moves upward under the drive of the two peaks, and more details will be given in the cases of this section.

4.3.1. Effect of the inter-bubble distance

Cases 1–3 The interaction between horizontal in-phase bubbles and the free surface with $\gamma_{\rm f} = 1.0$, $b = 1.6$, $b = 1.8$, and $b = 2.0$.

The crown spikes induced by horizontal in-phase bubbles with $\gamma_{\rm f} = 1.0$ and different b are simulated numerically, as depicted in Fig. 12. The dimensionless times are selected at the time of the initial formation of crown, at the time when crown rises to the level parallel to the distant quiescent water surface and at the moment when crown height equals valley height in Case 1. To further study the kinetic characteristic of the fluid domain, the corresponding velocity vectors in Case 1 are calculated at the same time (see Fig. 13).

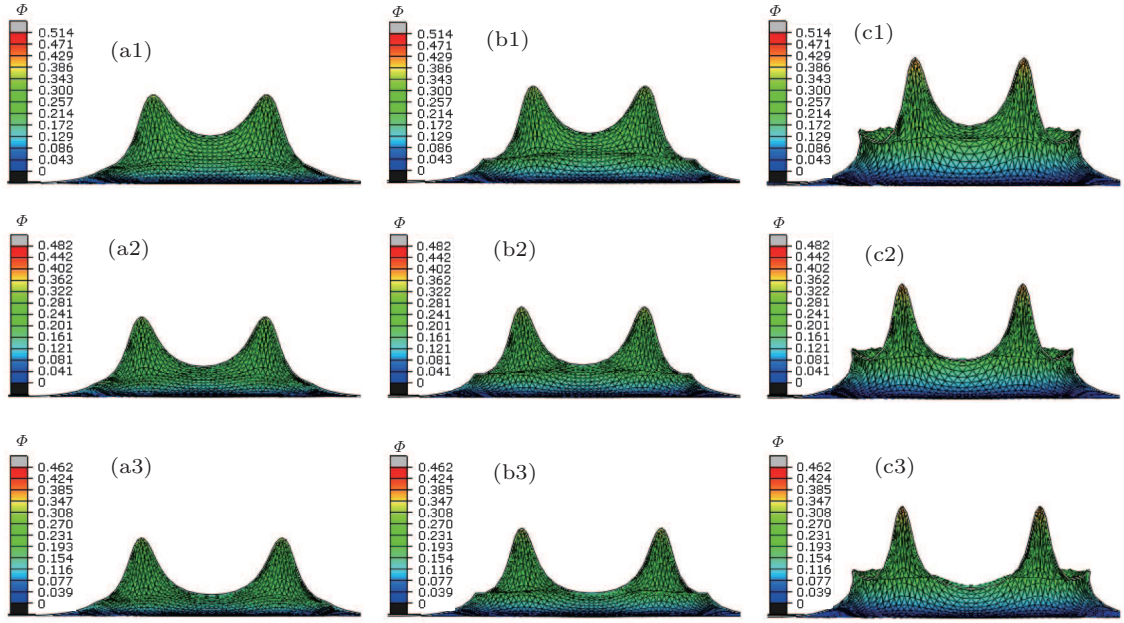


Fig. 12. (color online) Crown spike induced by bubbles at (a1) $T' = 2.196$, (a2) $T' = 2.2$, (a3) $T' = 2.218$, (b1) $T' = 2.513$, (b2) $T' = 2.585$, (b3) $T' = 2.605$, and (c1)–(c3) $T' = 3.5$ with $\gamma_{\mathrm{f}} = 1.0$, but different b.

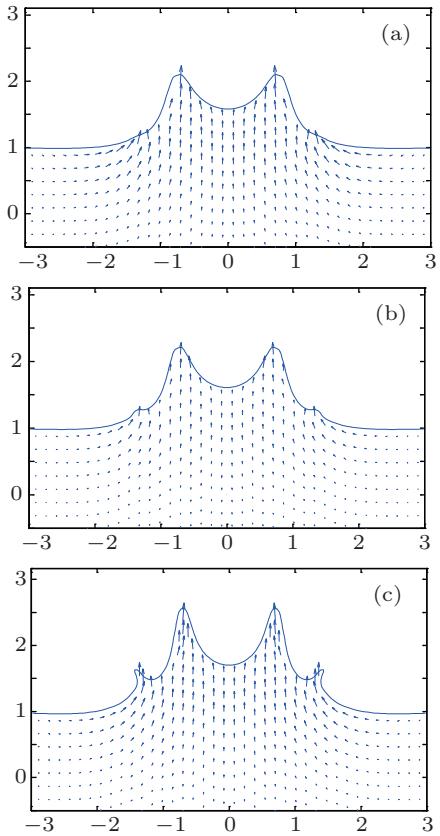


Fig. 13. (color online) Velocity vectors of the fluid domain at (a) $T' = 2.196$, (b) $T' = 2.513$, and (c) $T' = 3.5$.

In Figs. 12(a1)–12(a3), later occurrence of the crown phenomenon and a smaller valley height are observed for greater γ_{f}, and the corresponding velocity vectors of the fluid domain explain the upward motion of the spike (see Fig. 13(a1)). Observing the velocity vectors of the peaks, both the rise in height and the reduction in width can be indicated and the peaks will move toward the center due to the velocity components in horizontal direction. Observe the velocity vectors of the crown position, it is assured that the crown phenomenon will be more evident. At the moment in Fig. 12(b), the rise in both peak height and valley height proceeds, the contraction in the peak width can be observed at the same time, and it can be seen that the crown rises faster than the valley in the three cases above. We note the same motion trend of the two peaks from Fig. 13(b1) and it is found that the crown continues to move upward with the tendency of crown extension. The forms of crown spike at the same instant are compared in Fig. 12(c), and the peaks gradually become slimmer and come closer. Notice the horizontal displacements of two-peak tips with different b in Fig. 14, the peaks mainly influenced by bubbles are in vertical motion without horizontal displacements at the expansion phase and at the collapse phase the interplay between the two peaks becomes larger while the bubbles affect the free surface less, resulting in a slight convergence of the two peaks toward the center line. It is noted that the two peaks converge more slowly and the horizontal displacements become smaller with the increase in b. Because of the larger upward velocity of the crown, the crown in Case 3 is even higher than the valley at this instant, and a groove can be seen between the peaks and the crown in all cases with different extents of the crown extension. The corresponding velocity vectors shown in Fig. 13(c1) indicate the proceeding ascent of the spike and the same motion trend of the peaks, the tips of the peaks move upward at a maximum speed and the crown comes second with continued

extension. By observing the evolution of the spike, the variation trends of peak height $H_{\rm m}$ and crown height $H_{\rm c}$ are similar to those in single-bubble cases, as shown in Figs. 15 and 16. It is noted that the reduction of b leads to a larger two-peak interplay, a greater peak height, an earlier occurrence of the crown, and a faster growth in the crown height.

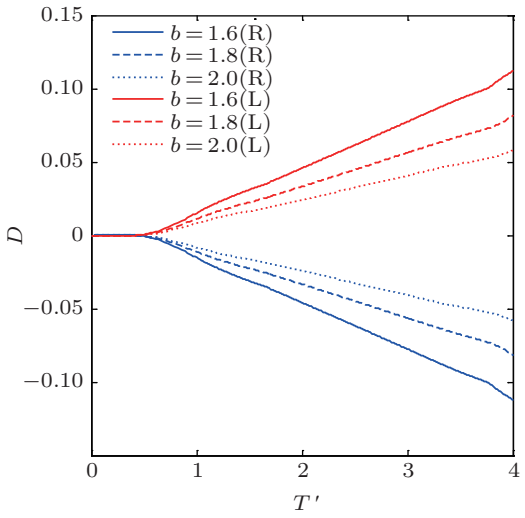


Fig. 14. (color online) Horizontal displacements of two-peak tips with different b.

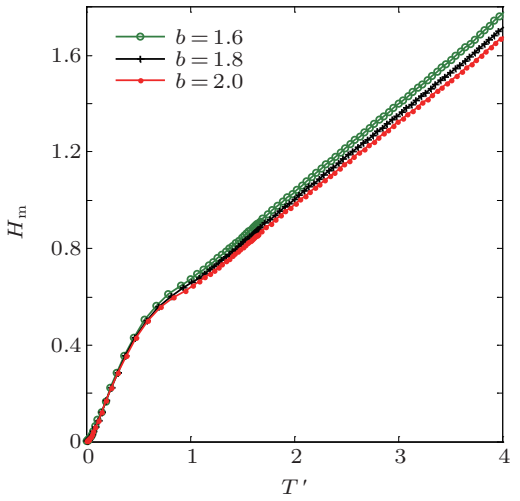


Fig. 15. (color online) Peak heights with different b.

The dimensionless inter-bubble distance b and the distance parameter $\gamma_{\rm f}$ are vital factors to different phenomena of free-surface spikes in two-bubble cases. The effect of the dimensionless inter-bubble distance b is investigated in the former three cases. Differing from the single-bubble cases, we note that the variation of crown width W with time is influenced by the existence of another bubble and that a valley between peaks appears due to the two-peak interplay. Comparisons are made in Figs. 17 and 18.

The variation of crown width W with time is illustrated in Fig. 17. Differing from the single-bubble cases, the curve of width–time does not slope down, but keeps the upslope due to the interplay of the two peaks. If b increases, the crown forms later with a larger initial width and the growth in crown width is slower as a result of less impact between the peaks, leading to a curve crossover at some point. We also note that crown extension is easier to appear for smaller b, thus reaching a greater width eventually. Figure 18 shows the variation of valley height $H_{\rm v}$ with time for the above three cases. We notice that all the curves first ascend and descend afterwards. If the impact occurs, then the increase in the valley height ensues. At the bubble expansion phase, the valley moves upward due to the vertical speed gained, and at the collapse phase, the valley falls by gravity. However, the continuous ascent of the peaks restrains the valley from moving downward and drives the valley to rise again after the impact. It can be seen that the valley height $H_{\rm v}$ increase more slowly during the expansion phase and then decreases more during the collapse phase with a greater b, and that the increase speed of the valley height after the impact does not make much difference for the above three cases, all with a linear growth.

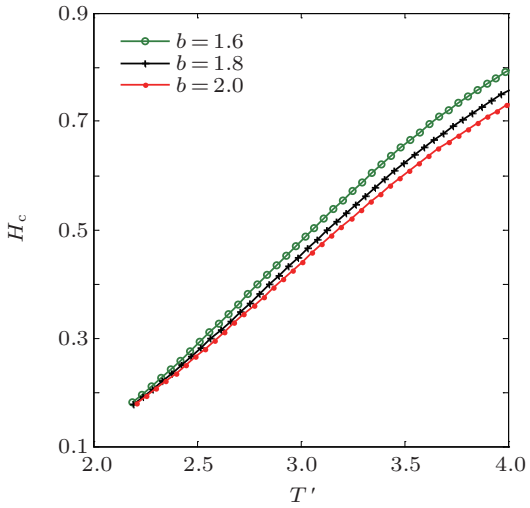


Fig. 16. (color online) Crown heights with different b.

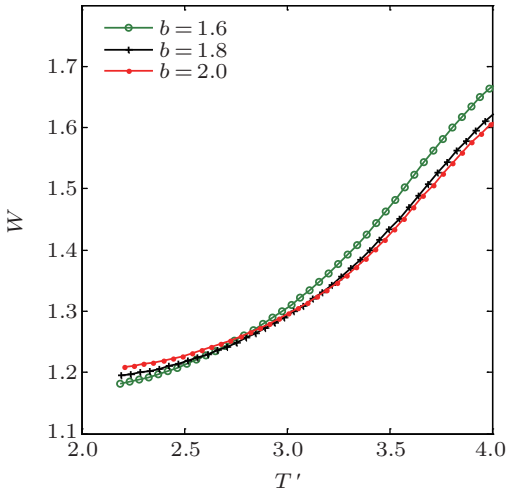


Fig. 17. (color online) Crown width with different b.

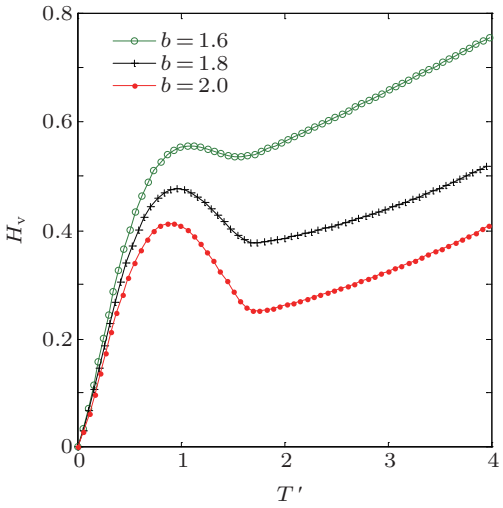


Fig. 18. (color online) Valley heights with different b.

As mentioned above, the interaction between bubbles makes the free-surface spike in the two-bubble cases different from that of the single-bubble cases. To understand the differences, the dimensionless impact time T'_j, the maximum vertical velocity of the peak tip $V_{m,\max}$, the crown height H_c, and the crown width W at $T' = 4$ are compared in Table 2.

Compare T'_j, the longer impact time in two-bubble cases states the suppression by the other bubble and a greater inhibition is expected with the reduction of b, giving rise to a longer impact time and accordingly higher spike owing to the longer time of the interaction. The maximum vertical velocity of the peak tip $V_{m,\max}$ is compared and a greater vertical velocity is obtained in two-bubble cases, which indicates a higher peak. At time $T' = 4$, the crown height H_c and width W in two-bubble cases are greater than those of the single-bubble cases. It is found that $V_{m,\max}$, H_c, and W all increase with the reduction of b. In summary, crown phenomena in two-bubble cases are clearer than those of single-bubble cases, especially for bubbles with smaller b.

Table 2. Comparison between single- and two-bubble cases.

	T'_j	$V_{m,\max}$	H_c	W
Single bubble	1.581	0.983	0.665	1.363
$b = 1.6$	1.682	1.079	0.791	1.664
$b = 1.8$	1.665	1.060	0.749	1.610
$b = 2.0$	1.653	1.047	0.730	1.605

4.3.2. Effect of the distance parameter

Cases 4 and 5 The interaction between horizontal in-phase bubbles and the free surface with $b = 1.6$, $\gamma_f = 1.1$ and 1.2.

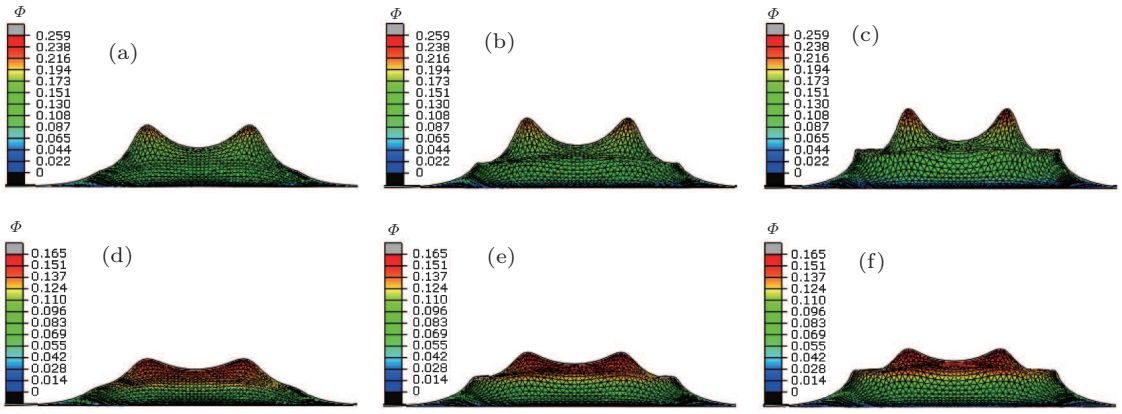


Fig. 19. (color online) Crown spike induced by bubbles at (a) $T' = 2.388$, (b) $T' = 2.87$, (c) $T' = 3.5$, (d) $T' = 2.768$, (e) $T' = 3.562$, and (f) $T' = 4$ with $b = 1.6$, but different γ_f.

To investigate the effect of the distance parameter, the free surface of Figs. 12(a1)–12(c1) is recomputed using $\gamma_f = 1.1$ and $\gamma_f = 1.2$. The selection of typical dimensionless instants in Case 4 is the same as that of Case 2. However, the third moment in Case 5 is selected at $T' = 4$ because of much later occurrence of the crown. The numerical results are presented in Fig. 19 to make a comparison with the free-surface profiles in Figs. 12(a1)–12(c1).

The profiles in Fig. 19 show that crown occurs later and peaks protrude less if γ_f increases. Similar to the phenomenon in Case 1, the peaks produce a displacement toward the center and the motion trend is the same as that in Fig. 14. As shown in Fig. 20, at $b = 1.6$, the larger the γ_f, the weaker the coupling effect between the bubbles and the free surface, so the motion of the peaks is influenced more by each other to produce greater horizontal displacements. When it comes to $T' = 3.500$, a groove appears between the peaks and the crown in both Case 1 and Case 4, all with crown extension. Nevertheless, crown extension still cannot be observed at $T' = 4.000$ in Case 5. The variation trends of peak height H_m, crown height H_c, and crown width W are similar to those in single-bubble

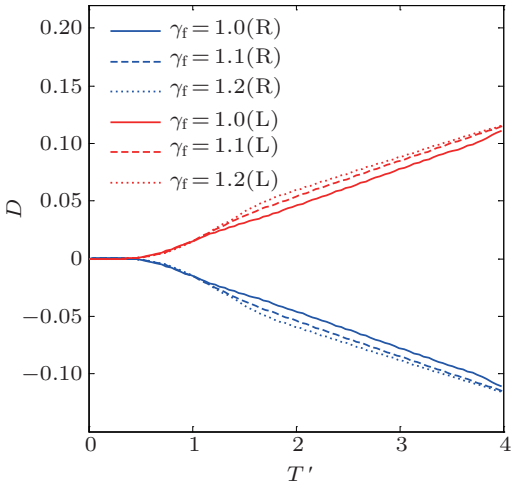


Fig. 20. (color online) Horizontal displacements of two-peak tips with different γ_f.

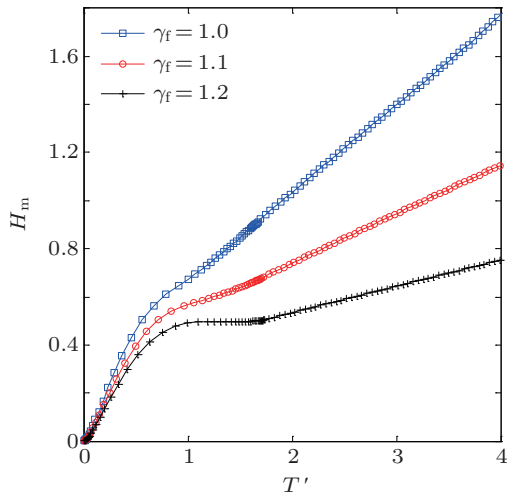


Fig. 21. (color online) Peak heights with different γ_f.

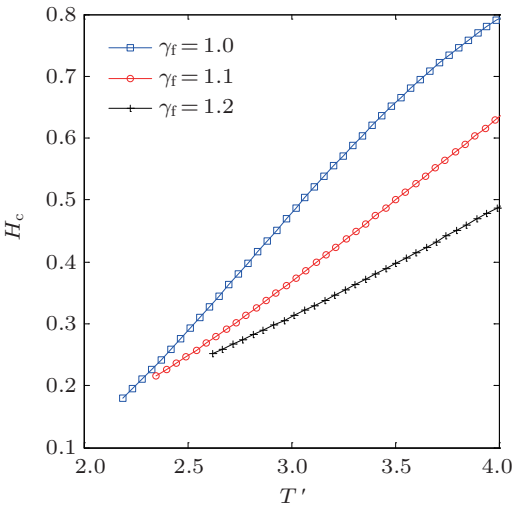


Fig. 22. (color online) Crown heights with different γ_f.

cases, as illustrated in Figs. 21–23, and the same conclusions can also be made. The variation trend of the valley heights in Fig. 24 is the same as that in Fig. 18. When bubbles are initiated 1.6 R_m apart, if γ_f increases, the valley height H_v increases more slowly during the expansion phase and then decreases more during the collapse phase, while the increase speed of the valley height after the impact does not make big difference for these three cases, all with a linear growth.

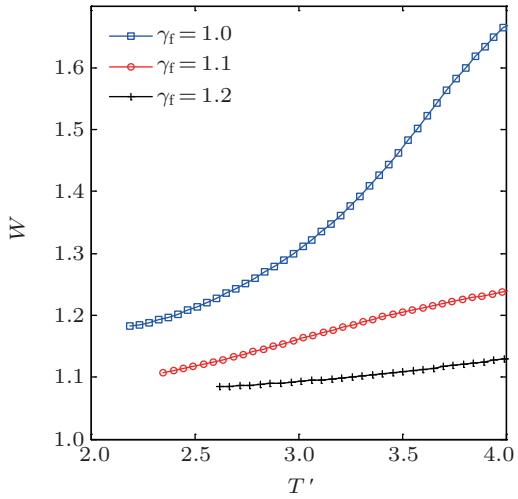


Fig. 23. (color online) Crown width with different γ_f.

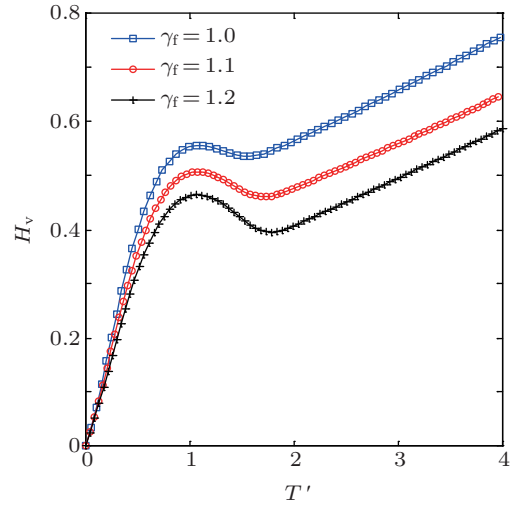


Fig. 24. (color online) Valley heights with different γ_f.

5. Conclusion

Three-dimensional numerical investigation has been carried out for the crown spike generated by one bubble or a horizontal line of two in-phase bubbles. Based on potential flow theory, a 3D numerical model is established to simulate the evolution of both the bubble and the free surface. The validity of the model in this paper is tested by comparing numerical and experimental results, for both the spike shapes and the motion trends are in accordance. The crown spikes in both single- and two-bubble cases have been simulated numerically to investigate the effects of the distance parameter and the dimensionless inter-bubble distance. The following conclusions are obtained.

(i) The distance parameter γ_f is the key factor to different motion features of crown spike. When the distance parameter $\gamma_f \in [1.0, 1.2]$, the coupling effect between gas bubbles and free surface increases with the reduction of γ_f, resulting in greater values of peak height H_m, crown height H_c, and crown width W.

(ii) The interplay between two horizontal in-phase bubbles strengthens the bubble-free-surface coupling effect, and the two peaks move inward to the center line due to the attraction of each other. When the dimensionless inter-bubble distance $b \in [1.6, 2.0]$ with the same γ_f, the values of the peak height H_m, the crown height H_c, the crown width W, and the valley height H_v increases as b decreases, so do the horizontal displacements of the two-peak tips toward the center line.

(iii) When the distance parameter $\gamma_f \in [1.0, 1.2]$ with the same b, the values of the peak height H_m, the crown height H_c, the crown width W, and the valley height H_v increase with the reduction of γ_f, while the horizontal displacements of the two-peak tips decrease simultaneously.

Acknowledgement

The authors acknowledge a PhD candidate of Harbin Engineering University—Cui Pu for help in conducting experiments.

References

[1] Gibson D C 1968 *The Third Australasian Conference on Hydraulic and Fluid Mechanics*, November 25–29, 1968 Sydney, Australia, p. 210
[2] Chahine G L 1977 *Trans. ASME Ser. I. J. Fluid Eng.* **99** 708
[3] Blake J R and Gibson D C 1981 *J. Fluid Mech.* **111** 123
[4] Voinov O V and Voinov V V 1975 *Sov. Phys. Dokl.* **20** 179
[5] Blake J R, Taib B B and Doherty G 1987 *J. Fluid Mech.* **181** 197
[6] Zhang A M and Yao X L 2008 *Acta Phys. Sin.* **57** 1662 (in Chinese)
[7] Wang Q X, Yeo K S, Khoo B C and Lam K Y 1996 *Theoret. Comput. Fluid Dynamics* **8** 73
[8] Wang Q X, Yeo K S, Khoo B C and Lam K Y 1996 *Comput. Fluids* **25** 607
[9] Zhang A M, Yang W S, Huang C and Ming F R 2013 *Comput. Fluids* **71** 169
[10] Tomita Y and Kodama T 2001 *IUTAM Symposium on Free Surface Flows,* July 10–14, 2000 Birmingham, UK, p. 303
[11] Robinson P B, Blake J R, Kodama T, Shima A and Tomita Y 2001 *J. Appl. Phys.* **89** 8225
[12] Pearson A, Cox E, Blake J R and Otto S R 2004 *Eng. Anal. Bound. Elem.* **28** 295
[13] Connor J G and Higdon C E 1996 NSWCDD/TR-96/178
[14] Kolsky H, Lewis J P, Sampson M T, Shearman A C and Snow C I 1949 *Proc. R. Soc. Lond. A* **196** 379
[15] Longuet-Higgins M S 1983 *J. Fluid Mech.* **127** 103
[16] Rogers J C W and Szymczak W G 1997 *Phil. Trans. R. Soc. Lond. A* **355** 649
[17] Zhang A M, Wang C, Wang S P and Cheng X D 2012 *Acta Phys. Sin.* **61** 084701 (in Chinese)
[18] Li S, Zhang A M and Wang S P 2013 *Acta Phys. Sin.* **6**2 194703 (in Chinese)
[19] Dadvand A, Shervani-Taba M T and Khoo B C 2011 *Int. J. Adv. Manuf. Technol.* **56** 245
[20] Fong S W, Adhikari D, Klaseboer E and Khoo B C 2008 *Exp. Fluids* **46** 705
[21] Dadvand A, Khoo B C, Shervani-Tabar M T and Khalilpourazary S 2012 *Eng. Anal. Bound. Elem.* **36** 1595
[22] Newman J N 1977 *Marine Hydrodynamics* (1st edn.) (London: MIT Press) p. 131
[23] Cole R H 1948 *Underwater Explosions* (1st edn.) (Princeton, NJ: Princeton University Press) p. 164
[24] Rungsiyaphornrat S, Klaseboer E, Khoo B C and Yeo K S 2003 *Comput. Fluids* **32** 1049
[25] Li Z R, Sun L, Zong Z and Dong J 2012 *Acta Mech. Sin.* **28** 51
[26] Zhang A M and Yao X L 2008 *Acta Phys. Sin.* **57** 339 (in Chinese)
[27] Wilkerson S A 1990 *A Boundary Integral Approach to Three-Demensional Underwater Explosion Bubble Dynamics* (Ph.D. Dissertation) (Baltimore: Johns Hopkins
[28] Klaseboer E, Fernandez C R and Khoo B C 2009 *Eng. Anal. Bound. Elem.* **33** 796
[29] Lee M, Klaseboer E and Khoo B C 2007 *J. Fluid Mech.* **570** 407
[30] Buogo S and Cannelli G B 2002 *J. Acoust. Soc. Am.* **111** 2594